ACS OMEGA

http://pubs.acs.org/journal/acsodf

Article

Facile Fabrication of Polyaniline/Pristine Graphene–Bacterial Cellulose Composites as High-Performance Electrodes for Constructing Flexible All-Solid-State Supercapacitors

Huijun Tan, Ding Xiao, Rahul Navik, and Yaping Zhao*

Cite This: *ACS Omega* 2021, 6, 11427–11435

Read Online

ACCESS | Metrics & More | Article Recommendations

ABSTRACT: A novel structured composite of polyaniline/pristine graphene (PG)–bacterial cellulose (BC) as electrodes fabricated in a facile approach and the foldable all-solid-state supercapacitors with high performance were reported in this work. The shear mixed PG–BC substrate was fixed with in situ polymerized polyaniline as a solder, improving its charge carrier transfer rate and cycling stability, while hydrophilic BC greatly improved the ion diffusion rate of the electrolyte. The as-prepared composites possessed a high areal capacitance of 3.65 F/cm^2 at 5 mA/cm^2, and the electrode was able to be bent into different shapes without fracture. The assembled all-solid-state supercapacitor was flexible and exhibited excellent areal capacitance of 1389 mF/cm^2, energy density of 9.80 mWh/cm^3, and 89.8% retention of its initial capacitance after 5000 cycles at a current density of 2 mA/cm^2. The composite is expected to have applications in making flexible supercapacitors applied in wearable devices.

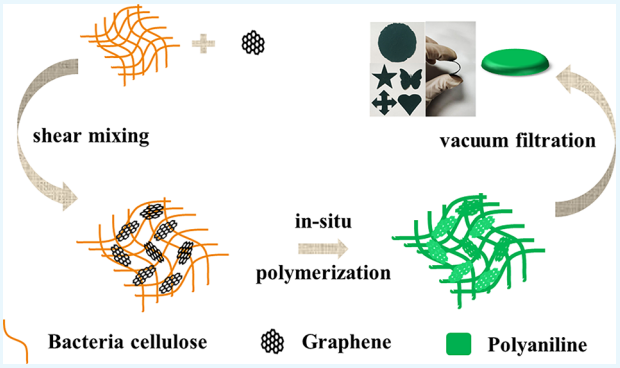

1. INTRODUCTION

Nowadays, the increasing energy demand has drawn extensive attention towards energy storage devices, including rechargeable batteries and supercapacitors. The supercapacitor is an efficient energy storage device because of its high power density, long cycling life, and fast charging rate.[1] The fast development of touch screens and wearable communication devices has promoted the demand for flexible and lightweight supercapacitors[2−4] because they could be folded and cut into different shapes without damaging their original electrochemical performances.[5] In fabricating flexible supercapacitors, flexible substrates such as stainless steel fabric and polyethylene terephthalate substrates[6,7] were often applied. However, these substrates cannot meet the demand for lightweight wearable devices since they suffer from either heavyweight or low conductivity.

Recently, graphene has drawn much attention in the production of flexible energy storage devices because of its high electrochemical activity and short path of ion transport.[8] In general, graphene was often utilized together with pseudocapacitive materials such as polyaniline (PANI)[9,10] to overcome its low capacitance in preparing flexible electrodes for supercapacitors.[11−15] However, the contradiction between the high loading amount of active components for achieving a high areal capacitance and the low loading for keeping the flexibility of the composite film has been a big issue. Also, the graphene used in the published studies had low electrical conductivity and capacitive performance[12−16] because it was mostly in the form of reduced graphene oxide (rGO) having a large number of defects in the structure. Thus, adopting suitable substrates and graphene with high electrical conductivity is still highly desired in fabricating flexible and high-performance supercapacitors.

Pristine graphene (PG) exfoliated from graphite in supercritical CO_2 had a higher electrical conductivity than rGO because it maintained its original lattice structure.[17] However, the exfoliated PG was poor in forming flexible films itself because it consisted of a few layers.[11] Bacterial cellulose (BC) is a good substance modifying PG to form a flexible substrate as it consists of ultrathin nanofibers with a diameter of less than 100 nm[18−20] and has abundant hydroxyl functional groups on the fiber surface, which allow fast diffusion of aqueous electrolytes and strong absorptivity.[21−23] Thus, the PANI/PG–BC composite would have good electrochemical performance and flexibility. However, the PANI had poor absorption and distribution in the PANI/PG–BC composite made by the filtration method of PANI onto the surface of the

Received: January 25, 2021
Accepted: April 16, 2021
Published: April 23, 2021

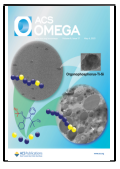

https://doi.org/10.1021/acsomega.1c00442
ACS Omega 2021, 6, 11427–11435

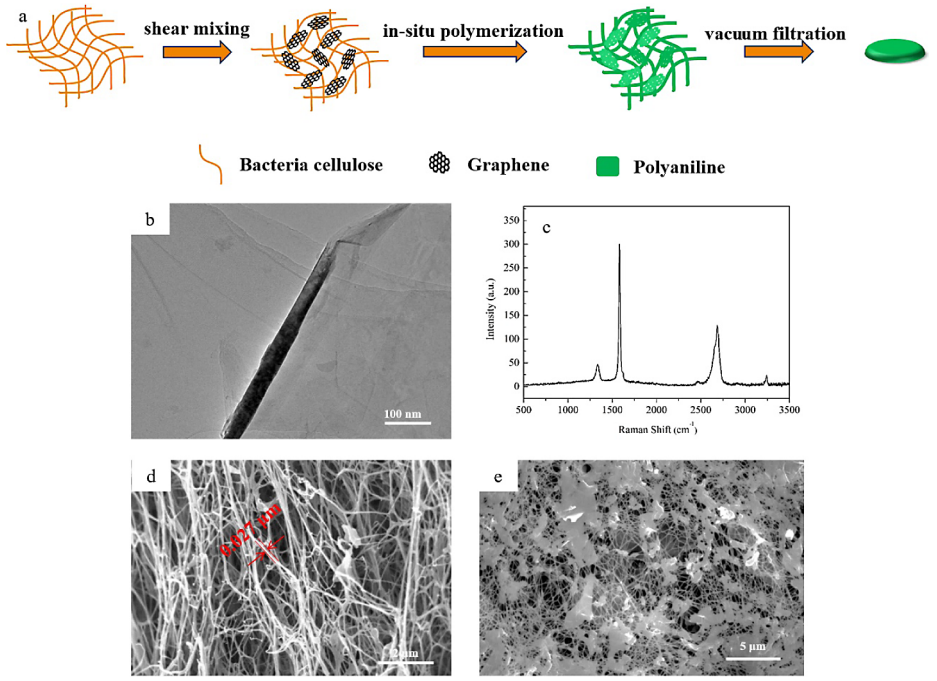

Figure 1. (a) Schematic illustration of the synthesis of the PANI/PG−BC composite, (b) TEM image of PG, (c) Raman spectra of graphene, (d) SEM image of BC, and (e) SEM image of the PG−BC substrate.

BC network.[14,24] In this paper, we first prepared a PG−BC substrate with a network structure by mixing PG with BC on a microscopic scale, whereafter, the PANI/PG−BC composite film with excellent flexibility was fabricated via the in situ polymerization of PANI on the surface of the PG−BC substrate, in which PG was fixed tightly on the BC surface via PANI binding. The influences of the loading amount and the different mass ratios between PG and PANI on the morphology, structure, and electrochemical performance of the electrodes were investigated. Also, the assembled symmetric all-solid-state supercapacitor was evaluated in a two-electrode test system. The characterization and analysis of the samples confirm that a novel structured PANI/PG−BC composite was fabricated, and the assembled all-solid-state supercapacitors with high performance were highly flexible and foldable.

2. RESULTS AND DISCUSSION

2.1. Morphology and Structure. The process of the fabrication of the PANI/PG−BC composite is shown in Figure 1a. The composite was prepared via shear mixing of PG and BC to form a substrate followed by the in situ polymerization of the aniline monomer.

The characterization results of PG, BC, and the PG−BC substrate are shown in Figure 1b−e. The TEM image shown in Figure 1b suggested that the graphene sheets were semi-transparent, wrinkled, and scrolled on edge, which implied that the PG consisted of an ultrathin structure. Also, a sharp 2D peak located at 2689 cm^{-1} in the Raman spectrum (Figure 1c) and an intensity ratio of 2.32 between G and 2D peaks (I_G:I_{2D}) suggested that the as-prepared PG was few-layer.[25] Pure BC constituted of cross-linked BC fibers with a diameter of 20−30 nm, as shown in Figure 1d. It can be seen from Figure 1e that the interlaced graphene was embedded and confined on the surface of the BC network in the PG−BC substrate.

The influence of the PANI loading amount and PG content on the morphology and structure of PANI/PG−BC composite was investigated. In each composite, 50 mg of BC mass was utilized. Initially, a suitable range of the loading amount of PANI was investigated to maintain the flexibility of the composite film. The loading amount was studied by changing the concentration of the aniline monomer in a reaction system from 0.025 to 0.15 mol/L without adding PG. The samples were named PANI−BC1, PANI−BC2, PANI−BC3, and PANI−BC4 corresponding to different aniline monomer concentrations of 0.025, 0.05, 0.1, and 0.15 mol/L, respectively. As shown in Figure 2, PANI was adsorbed onto the surface of BC and leads to an increase in the fiber diameter. Both the fiber diameter and the loading amount increased with an increase in the aniline monomer concentration. The PANI loading amounts of composites were 1.96, 2.59, 4.16, and 8.13 mg/cm^2 corresponding to the average fiber diameters of 0.07, 0.11, 0.17, and 0.24 μm, respectively. A large amount of aniline

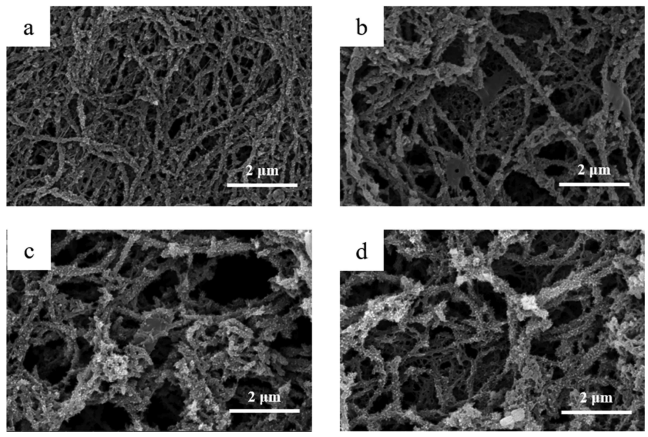

Figure 2. SEM images of PANI−BC fibers with an aniline monomer concentration of (a) 0.025 mol/L, (b) 0.05 mol/L, (c) 0.1 mol/L, and (d) 0.15 mol/L.

https://doi.org/10.1021/acsomega.1c00442
ACS Omega 2021, 6, 11427−11435

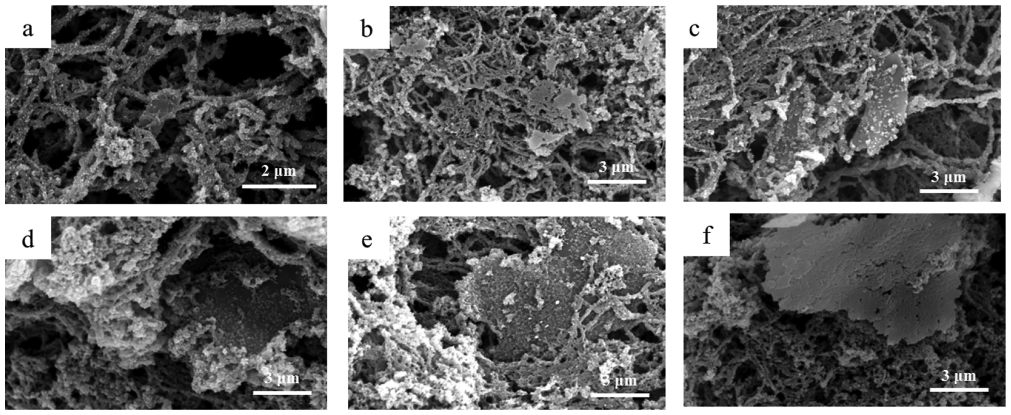

Figure 3. SEM images of PANI/PG−BC composites with different graphene contents: (a) 0 wt %, (b) 1.25 wt %, (c) 2.5 wt %, (d) 5 wt %, (e) 10 wt %, and (f) 20 wt %.

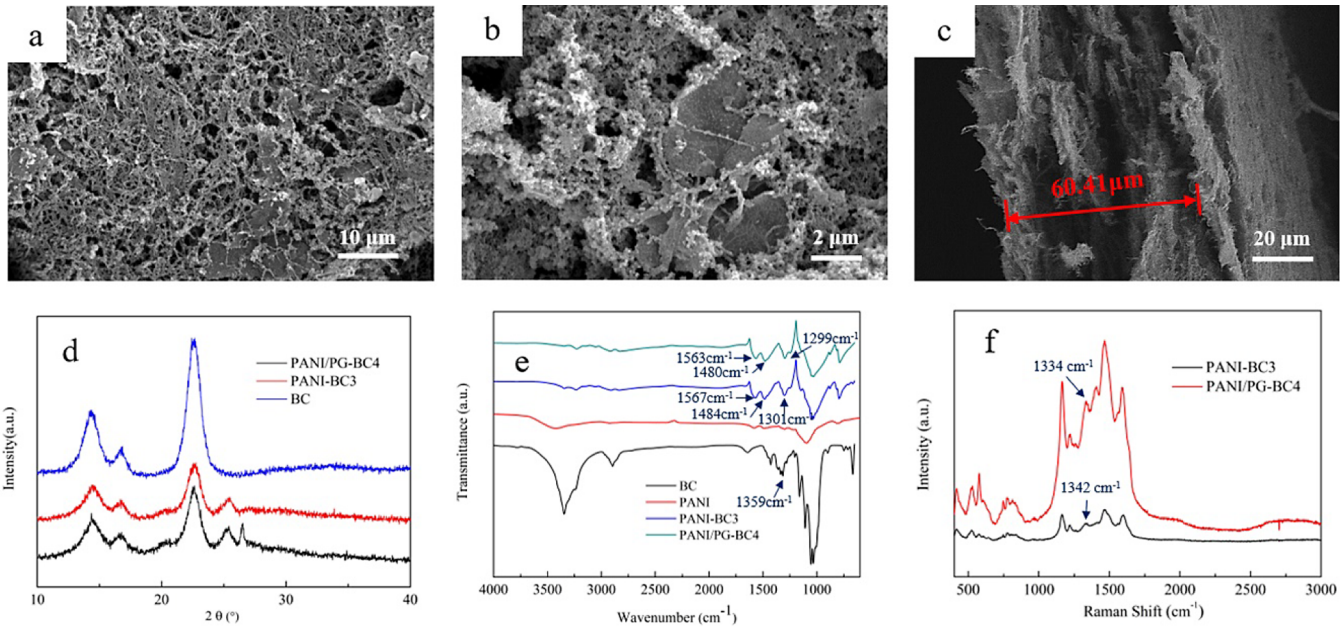

Figure 4. SEM images of the PANI/PG−BC4 composite with an aniline monomer concentration of 0.1 mol/L and a graphene content of 10 wt % at (a) low magnification and (b) high magnification, (c) SEM cross-sectional image of the PANI/PG−BC4 composite, (d) XRD diffraction patterns and (e) FTIR spectra of BC, PANI, PANI−BC3, and PANI/PG−BC4 composites, and (f) Raman spectra of PANI−BC3 and PANI/PG−BC4 composites.

monomer adsorbed onto the surface of the PG−BC network with an increase in the aniline monomer concentration, resulting in more active sites in a subsequent polymerization process. Therefore, the fiber diameter and loading amount increased. However, an increased fiber diameter would reduce the flexibility of the composite film because the excess aniline monomer tended to form nucleation in solution and polymerized into isolated PANI nanowire clusters,[26] as shown in Figure 2d. Therefore, an aniline monomer concentration of 0.1 mol/L was considered to be the optimal concentration.

The influences of the PG content on the morphology and structure of the samples were investigated at a fixed aniline monomer concentration of 0.1 mol/L. The as-prepared composites were named PANI/PG−BC1, PANI/PG−BC2, PANI/PG−BC3, PANI/PG−BC4, and PANI/PG−BC5, corresponding to the graphene mass contents of 1.25%, 2.5%, 5%, 10%, and 20% in the PG−BC substrate, respectively. When the PG content increased from 0 to 10 wt %, the amount of PG impounded into the BC network increased, as shown in Figure 3a−e. During the polymerization process, aniline monomer first adsorbed onto the surface of the PG and BC substrate via $\pi-\pi$ interactions and hydrogen bonding, forming nuclei for the subsequent polymerization process. Then, PANI grew along the surface of the PG and BC cosubstrate, covering the surface of both components. The interconnected BC network acted as a scaffold for PG distribution, and the polymerized PANI acted as the binding agent. Thus, the PG was fixed tightly with a flexible BC network with the help of PANI. The PG defined into the BC network increased the specific surface area of the composite network, thereby producing more surface area for the adsorption and distribution of PANI later, and meanwhile, the adsorbed PANI could prevent PG from aggregation. However, with an increase in the PG amount in PG−BC, the PG started to aggregate and stack on the top of the composite network, on which a small amount of PANI occurred. This implies that PANI could not cover the entire surface of the

https://doi.org/10.1021/acsomega.1c00442
ACS Omega 2021, 6, 11427−11435

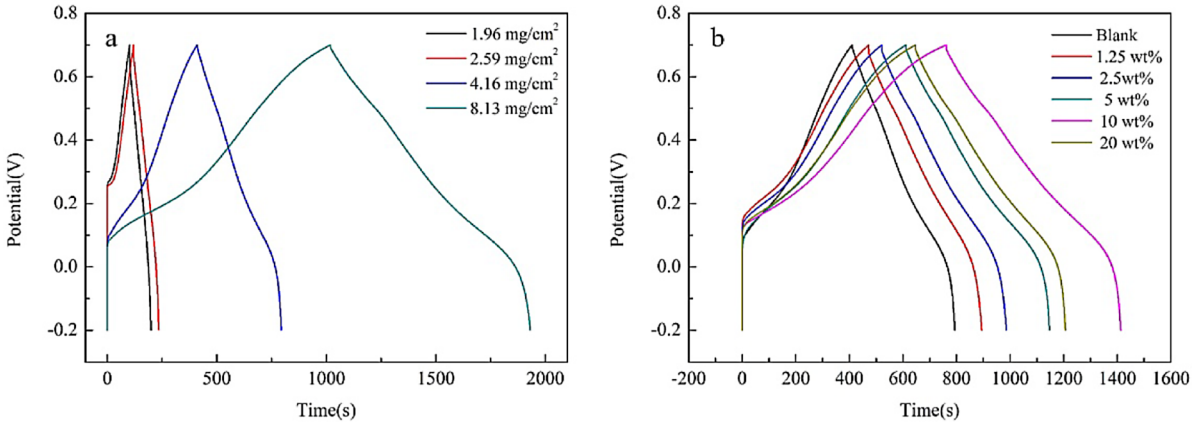

Figure 5. GCD curves of composites with (a) different loading amounts and (b) different graphene contents at a current density of 5 mA/cm^2.

composite network. Therefore, 10 wt % was considered as the optimal content in the PG−BC substrate.

The SEM image of the as-prepared PANI/PG−BC4 composite obtained under optimal conditions is displayed in Figure 4a−c. It can be seen that the surface of the BC network was covered with PG and PANI uniformly. The ultrathin nanofibers of BC not only served as a substrate that produced abundant cross-linked pore structures to impound PG into the network but also supplied PANI for better distribution and higher loading amount on the surface of the PG−BC substrate via $\pi-\pi$ interactions and hydrogen bonding in the entire composite. The cross-sectional SEM image of the PANI/PG−BC4 composite in Figure 4b showed the thickness of 60.41 μm and a porous structure inside the composite.

XRD analysis was further applied to characterize the combination of PG, BC, and PANI components. As shown in Figure 4c, the pure BC consisted of three major diffraction peaks at 2θ = 14.4°, 16.8°, and 22.6°, corresponding to the (1 1$^-$0), (110), and (200) lattice planes of cellulose I.[27] However, a new peak located at 2θ = 25.4° appeared in the diffraction pattern of the PANI−BC composite, which was mainly generated due to the deposition of PANI on the BC.[28] A weak and sharp peak located at 2θ = 26.6° in the PANI/G−BC composite was attributed to PG, showing the successful combination of PANI and PG onto the BC network.

Fourier transform infrared spectroscopy (FTIR) spectra of pure BC, PANI, PANI−BC3, and PANI/PG−BC4 composites are shown in Figure 4d. In the spectrum of pure BC, a broad band located at 3350 cm^{-1} represented the O−H stretching vibration, while the band positioned at 1359 and 1427 cm^{-1} belonged to the O−H in-plane deformation vibration. The band located at 2895.34 cm^{-1} was attributed to the aliphatic C−H stretching vibration, while the sharp bands at 1054, 1107, and 1161 cm^{-1} were ascribed to C−O−C stretching vibration, which was in accordance with the characteristic bands of pure BC.[27] The characteristic bands of pure PANI located at 1583, 1483, 1300, 1094, and 814 cm^{-1} represented the presence of the C═C stretching vibration of a quinoid structure and a benzene ring and the stretching vibration of C—N, C═N, and C—H, respectively.[29,30] In the case of PANI−BC, both characteristic bands of the BC and PANI were seen, and the O—H in-plane deformation vibration located at 1359 cm^{-1} was red-shifted to 1301 cm^{-1}, indicating a decreased bonding energy of hydrogen bonding between BC.[31] This suggested the combination of BC and PANI. The FTIR spectrum of PANI/PG−BC was similar to that of PANI−BC, except that the characteristic band of the O—H in-plane deformation vibration further red-shifted to 1299 cm^{-1} for the decreased bonding energy. Also, the bands of the C═C stretching vibration of the quinoid structure and benzene ring red-shifted from 1567 and 1484 cm^{-1} to 1563 and 1480 cm^{-1}, which mainly arose from the conjugational $\pi-\pi$ interactions between PANI and graphene.[32] The FTIR results confirmed the successful formation of the PANI/PG−BC composite. Moreover, the red-shift of the C—N stretching peak from 1342.64 to 1334.51 cm^{-1} in Raman spectra displayed in Figure 4f also evidenced the interactions between PANI and PG, which can facilitate the charge carrier transfer rate.[32]

2.2. Electrochemical Properties of Composites.

Electrochemical measurements of the electrodes were conducted at 25 °C using a three-electrode system, in which the specific capacitance of the composites prepared under various loading amounts and PG mass contents was first tested using the galvanostatic charge/discharge (GCD) method. The areal capacitance (C) was calculated from the discharge process according to the equation: $C = I \times \triangle t/(S \times \triangle V)$,[11] where I is the charge−discharge current (A), $\triangle t$ is the discharge time (s), S is the area of the testing electrode (cm^2), and $\triangle V$ is the potential charge in the discharging process (V).

Figure 5a shows the GCD curves of PANI−BC composites with different PANI loading amounts. It can be calculated that the areal capacitance was 0.55, 1.31, 2.15, and 5.12 F/cm^2 corresponding to the loading amounts of 1.96, 2.59, 4.16, and 8.13 mg/cm^2, respectively. The areal capacitance of the PANI−BC composites increased with increasing loading amount, which was mainly ascribed to the faradic pseudocapacitance property of PANI. However, when the loading amount was increased to 8.13 mg/cm^2, the composite film showed poor flexibility. Therefore, the loading amount of 4.16 mg/cm^2 corresponding to the aniline monomer concentration of 0.1 mol/L was chosen as the optimal condition. Figure 5b displays the influence of PG content on the areal capacitance. It can be seen that the areal capacitance increased with an increase in the PG content from 0 to 10 wt %, the capacitance of 2.15, 2.35, 2.61, 3.02, 3.65, and 3.15 F/cm^2 being corresponded to the PG content of 0, 1.25, 2.5, 5, 10 and 20 wt %, respectively. This can be attributed to the improved electrical conductivity of the composite film and the charge carrier transfer rate caused by graphene. Nevertheless, when the graphene content continuously increased to 20 wt %, the areal capacitance reduced, the reason of which would be

https://doi.org/10.1021/acsomega.1c00442
ACS Omega 2021, 6, 11427−11435

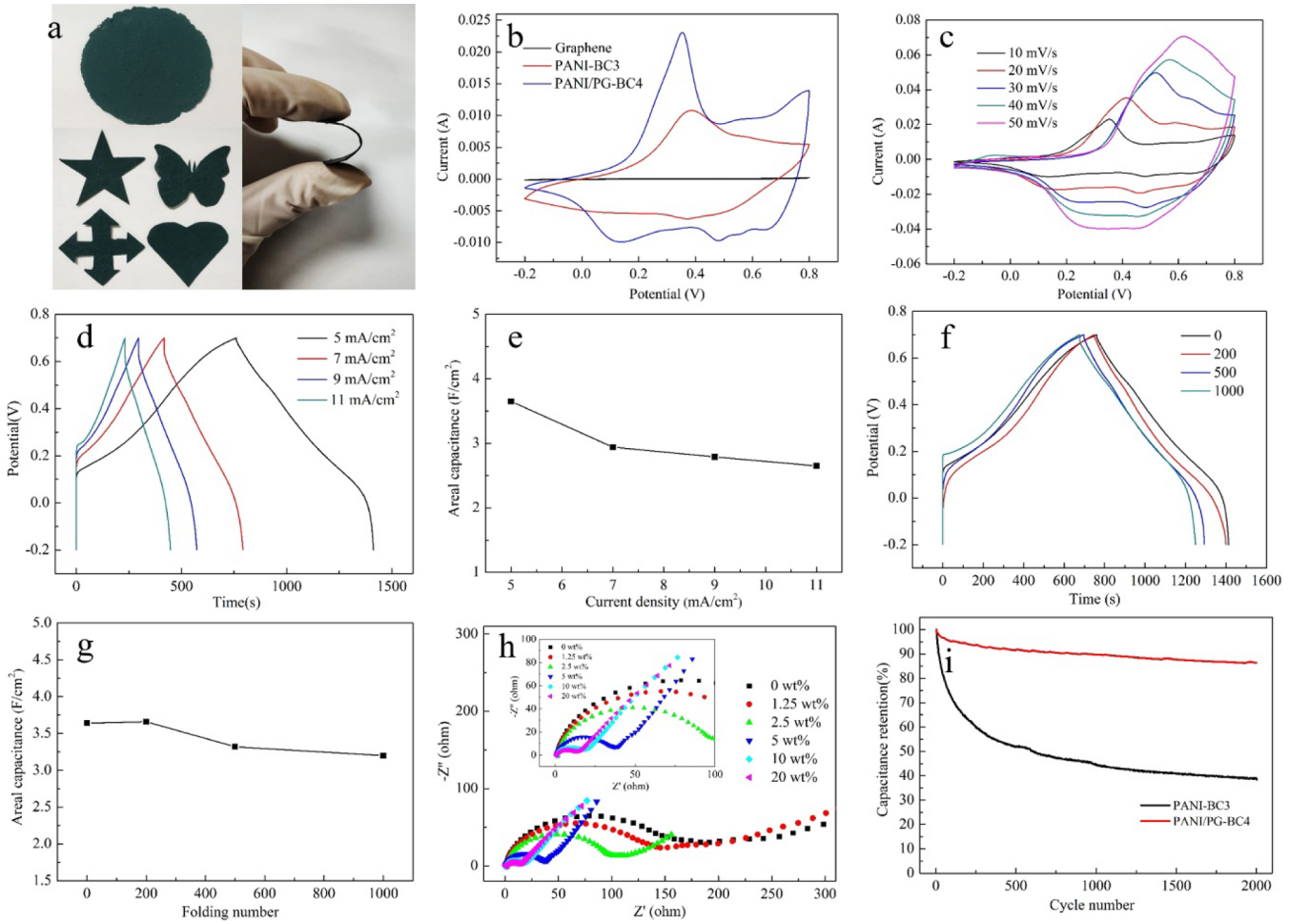

Figure 6. (a) Photograph of the PANI/PG−BC4 composite at an aniline monomer concentration of 0.1 mol/L and graphene content of 10 wt % as well as bending and cutting into different shapes. (b) CV curves of graphene, PANI−BC3, and PANI/PG−BC4 with the potential window of −0.2 to 0.8 V. (c) CV curves of the PANI/PG−BC4 composite with the potential window of −0.2 to 0.8 V at 10, 20, 30, 40, and 50 mV/s scan rate. (d) GCD curves of PANI/PG−BC4 at a current density of 5, 7, 9, and 11 mA/cm^2. (e) Specific capacitance of PANI/PG−BC4 at different current densities. (f) GCD curves of PANI/PG−BC4 after different folding times. (g) Areal capacitance of PANI/PG−BC4 after different folding times. (h) Nyquist plots of PANI−BC3 and PANI/PG−BC composites in the frequency range of 100 kHz to 0.01 Hz (the inset shows the enlarged plots of the high-frequency region). (i) Cycling stability of the PANI−BC3 and PANI/G−BC4 electrodes at 2 mA/cm^2 for 5000 cycles.

discussed later. Thus, the PG content of 10 wt % was considered as an optimal value.

The photograph and electrochemical performances of the PANI/PG−BC4 composite prepared under optimal conditions are shown in Figure 6. The photograph of the PANI/PG−BC4 composite film after freeze-drying, cutting, and bending is shown in Figure 6a. It can be seen that the as-prepared free-standing composite film showed good flexibility and could be cut and folded into the different desired angles and various shapes without damaging its original structure. Figure 6b shows the CV curves of PG, PANI−BC, and PANI/PG−BC4 composites. The CV curve of PG has a rectangular shape suggesting its double-layer capacitance character, while the CV curve of PANI showed redox peaks attributed to the transitions between the leucoemeraldine−emeraldine structure and the emeraldine−pernigraniline structure, respectively.[33,34] After the addition of graphene, the CV curve of the PANI/PG−BC4 composite possessed a larger integral area than PANI−BC3, suggesting the enhanced areal capacitance. The shape of the CV curve of PANI/PG−BC4 under various scan rates from 10 to 50 mV/s showed no significant change, confirming a quick response to redox reactions.[35] The areal capacitance of the composite reduced from 3.65 to 2.65 F/cm^2 as the current density increased from 5 to 11 mA/cm^2, and the capacitance retention was 72.6%, which was much higher than literature values, indicating the excellent rate capability of the composite.[36]

Figure 6f−g displays the capacitance change in the PANI/PG−BC4 composite under different folding times. The as-prepared composite maintained 87.9% of its initial capacitance after folding/release of 1000 cycles, with no distinction in the shape of the GCD curves. We can see from Figure 6h that the interfacial charge-transfer resistance (R_{ct}) of PANI/PG−BC composites decreased from 150 to 28 Ω as the graphene content increased from 0 to 20 wt %, demonstrating a better conductivity of the composite due to graphene addition, which considerably shortened the charge transmission pathways of electrons from the electrode to the current collector. The slope increase in Figure 6h also indicated a better diffusion rate of electrolyte into the electrode with graphene addition from 0 to 10 wt %. It should be noted that when the PG content was 20 wt %, the PANI/PG−BC5 composite formed a smaller slope than PANI/PG−BC4. It was mainly attributed to the fact that the aggregation of excess PG blocked the pathways for

https://doi.org/10.1021/acsomega.1c00442
ACS Omega 2021, 6, 11427−11435

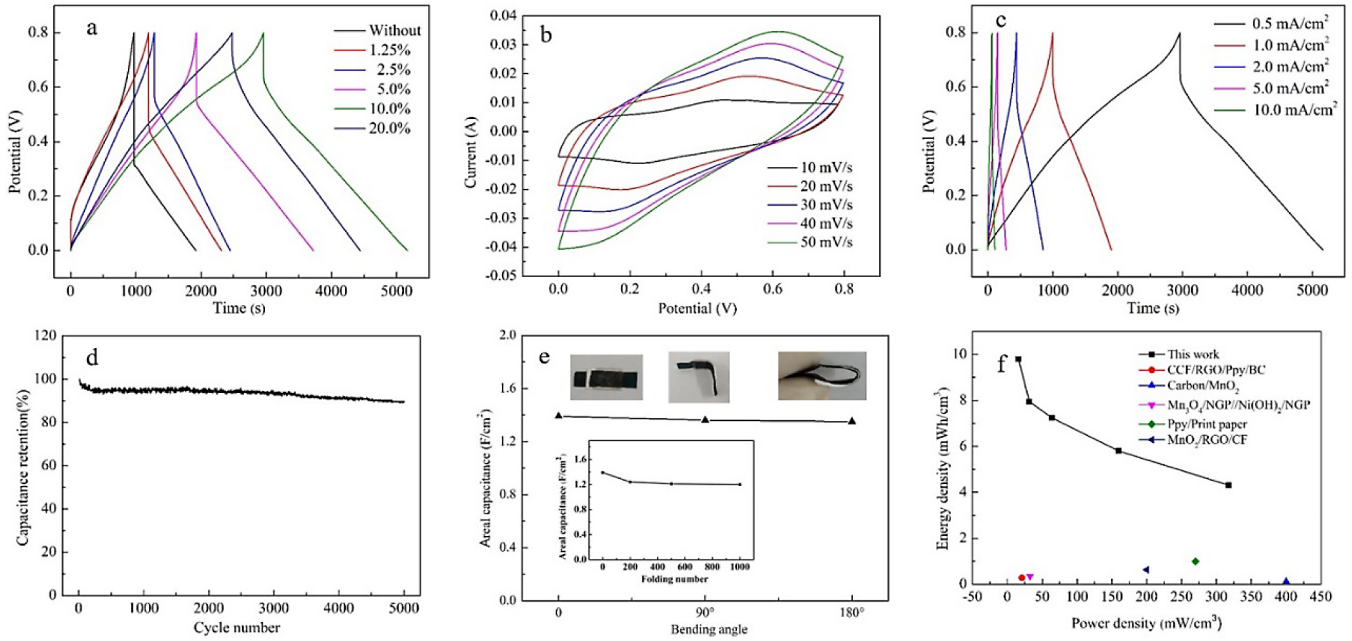

Figure 7. (a) GCD curves of supercapacitors based on PANI/PG−BC electrodes with various graphene contents at a current density of 0.5 mA/cm^2. (b) CV curves of the supercapacitor based on the PANI/PG−BC4 electrode at different scan rates. (c) GCD curves of the supercapacitor based on the PANI/PG−BC4 electrode at different current densities. (d) Cycling stability of the supercapacitor based on the PANI/PG−BC4 electrode at 2 mA/cm^2 for 5000 cycles. (e) Optical images and capacitance retention of devices at a different bending angle (the inset shows the capacitance retention of devices after repeated bending for 180° up to 1000 times. (f) Ragone plot of PANI/PG−BC4 devices. The volumetric energy densities and power densities reported for other supercapacitors[41−45] were added for comparison.

electrolyte penetration. The test of the cycling stability of composites under a current density of 2 mA/cm^2 proved that the areal capacitance maintained 92.1% after 5000 cycles for the PANI/G−BC4 composite, whereas only 38.3% for the blank PANI−BC3 composite.

2.3. Electrochemical Performance of All-Solid-State Supercapacitors. The symmetric all-solid-state supercapacitor devices were fabricated using PANI/PG−BC composites as electrodes without any additional flexible substrate and current collector. The GCD curves in Figure 7a showed that the areal capacitance of devices varied from 593 to 1389 mF/cm^2 when the graphene content increased from 0 to 10 wt %. However, the areal capacitance of the device with the graphene content of 20 wt % decreased to 1251 mF/cm^2, which might be attributed to the aggregation of excess graphene. Figure 7b−d shows the CV curves, GCD curves, and cycling stability of devices fabricated using PANI/PG−BC4 electrodes with an aniline monomer concentration of 0.1 mol/L and the PG content of 10 wt %. The CV curves showed no shape change with an increase in the scan rate, while the GCD curves showed that the areal capacitance decreased from 1389 to 612 mF/cm^2 when the current density increased from 0.5 to 10.0 mA/cm^2, and the device maintained 89.8% of its initial capacitance after 5000 cycles at a current density of 2 mA/cm^2. The maximum areal capacitance of the supercapacitor (1389 mF/cm^2) was higher than that of most of the literature studies.[37−40] Figure 7e shows the optical images and capacitance retention of the PANI/PG−BC4 device at different bending angles and the inset shows the capacitance retention after various bending times. It can be seen that the areal capacitance remained almost unchanged with different bending angles, while the areal capacitance decreased slightly in the first 200 cycles and remained almost unchanged afterward in bending. The capacitance retention was 86.3% after 1000 cycles in bending, showing its good stability. The maximum areal energy density of the device was 0.13 mWh/cm^2 with a power density of 0.20 mW/cm^2, and the device can maintain an energy density of 0.06 mWh/cm^2 at a power density of 4.0 mW/cm^2, which was superior to literature values.[14] For a better comparison, the volumetric energy density and power density were calculated and Figure 7f displayed the results of PANI/PG−BC4 devices as well as literature values. It can be seen that the maximum energy density and power density of the device were 9.80 and 317.14 mW/cm^3, respectively, which were much higher than other reports.[41−45]

3. CONCLUSIONS

A facile approach was developed to fabricate a novel structured PANI/PG−BC composite, in which PG was confined into the BC network. The PG and PANI distributed uniformly on the composite and fixed tightly to each other with BC. The PANI not only provided the faradic pseudocapacitance but also acted as a binding agent to fix PG onto the surface of the BC fiber. The cross-linked PG on the BC surface greatly improved the conductivity of the substrate and decreased the charge transfer resistance, thus improving the carrier transfer rate. Also, the PG and PANI dropping out from the PG−BC could be prevented during the long cyclic charge and discharge process and the PANI loading amount could be increased. Therefore, the as-prepared composites with high flexibility presented a high areal capacitance of 3.65 F/cm^2 at the current density of 5 mA/cm^2, and the capacitance retention of the electrode was 92.1% after 5000 cycles at a current density of 2 mA/cm^2. The assembled foldable all-solid-state supercapacitor exhibited an excellent areal capacitance of 1389 mF/cm^2 and an energy density of 9.80 mWh/cm^3. The composite is expected to have

https://doi.org/10.1021/acsomega.1c00442
ACS Omega 2021, 6, 11427−11435

applications in making flexible supercapacitors applied in wearable devices

4. EXPERIMENTAL

4.1. Materials. Graphite powder (99.85%, CP), aniline (AR), ammonium persulfate (AR), sulfuric acid (GR), and ethanol (≥99.5%) were purchased from Sinopharm Chemical Reagent Co., Ltd., Shanghai, China. BC was purchased from Hainan Yida Food Industry Co., Ltd. Carbon dioxide (99.9%) was purchased from Shanghai High-Tech Co., Ltd., China.

4.2. Preparation of the PG and PG−BC Substrate. PG was prepared via exfoliation of graphite in supercritical carbon dioxide using a shear mixer, according to a previously published paper.[17] The as-exfoliated graphene was collected in ethanol and separated via centrifugation at 3000 rpm for 15 min. The BC was put into deionized water and sheared using a mechanical homogenizer (Shanghai Angni Instruments Co., Ltd.) at 6000 rpm for 20 min to form a homogeneous suspension. Then, a PG−BC substrate was prepared by mixing a certain amount of BC suspension with PG suspension with a shear mixer at 6000 rpm for 30 min and subsequential stood to let PG be confined into the network of BC.

4.3. Preparation of PANI/PG−BC Composites. The PANI/PG−BC composite was prepared via in situ polymerization of aniline on the surface of the PG−BC substrate. Typically, a certain amount of aniline and H_2SO_4 were added into the PG−BC suspension and stirred for 1 h to allow aniline adsorb on the surface of the PG−BC substrate. Then, the system was transferred into an ice bath. The corresponding amount of ammonium peroxydisulfate (APS) was dissolved in 100 mL of ethanol−water (20 wt %) and injected into the reaction system using a syringe pump at a flow rate of 200 mL/h. After polymerization for 6 h, the reaction product was processed in series by vacuum filtrating, ethanol washing, deionized-water washing, and freeze-drying overnight to obtain the PANI/G−BC composite.

4.4. Fabrication of Symmetrical All-Solid-State Supercapacitors. The symmetrical flexible supercapacitors were assembled in a sandwiched structure using the as-prepared composite film as two electrodes. The PANI/PG−BC composite films were cut into the size of 1 × 3 cm^2 and immersed into the polyvinyl alcohol (PVA)/H_2SO_4 electrolyte gel for 30 min. Filter paper was used as a separator between the two electrodes. The as-prepared supercapacitors were put inside the fume hood at room temperature for 12 h to vaporize the excess water.

4.5. Characterization. The PG concentration (mg/mL) and PANI loading amount (mg/cm^2) were analyzed via a weighing method. The as-prepared samples were characterized using a field-emission scanning electron microscope (FE-SEM, Nova Nano-SEM 450, FEI Company, USA), an X-ray diffractometer (XRD, D8 Advance, Brock, Germany), a transmission electron microscope (TEM, JEM-2100 JEOL Ltd., Japan), Raman spectroscopy (DXR), and FTIR (Spectrum 100, Perkin Elmer, Inc., USA).

4.6. Electrochemical Measurements. Electrochemical measurements of the individual electrode and all-solid-state supercapacitors were conducted using a CHI 660E electrochemical workstation (Shanghai Chenhua Instrument Co., LTD, China) at 25 °C. A three-electrode system was employed in 1 M aqueous H_2SO_4 electrolyte, in which a saturated calomel electrode (SCE) and a Pt electrode were used as the reference and counter electrode, respectively. In the three-electrode test, the cyclic voltammetry (CV) curves were carried out from −0.2 to 0.8 V at the scanning rates of 10, 20, 30, 40, and 50 mV/s, respectively; GCD tests were measured at the current densities of 5, 7, 9, and 11 mA/cm^2 with a scanning range of −0.2 to 0.7 V, respectively; electrochemical impedance spectra (EIS) was recorded at an amplitude of 5 mV in a frequency ranging from 0.01 Hz to 100 kHz. The cycling stability was tested using a LAND-CT2001A workstation (Wuhan Lanhe Electronic Co., LTD, China) with charge−discharge cycling at a current density of 2 mA/cm^2 for 5000 cycles. The symmetrical all-solid-state supercapacitor was assembled using two-hybrid materials as electrodes and H_2SO_4/PVA as an electrolyte, respectively, and was measured in two-electrode configurations.

AUTHOR INFORMATION

Corresponding Author

Yaping Zhao − *School of Chemistry and Chemical Engineering, Frontiers Science Center for Transformative Molecules, Shanghai Jiao Tong University, Shanghai 200240, China*; orcid.org/0000-0001-5682-3370; Email: ypzhao@sjtu.edu.cn

Authors

Huijun Tan − *School of Chemistry and Chemical Engineering, Frontiers Science Center for Transformative Molecules, Shanghai Jiao Tong University, Shanghai 200240, China*

Ding Xiao − *School of Chemistry and Chemical Engineering, Frontiers Science Center for Transformative Molecules, Shanghai Jiao Tong University, Shanghai 200240, China*

Rahul Navik − *School of Chemistry and Chemical Engineering, Frontiers Science Center for Transformative Molecules, Shanghai Jiao Tong University, Shanghai 200240, China*

Complete contact information is available at: https://pubs.acs.org/10.1021/acsomega.1c00442

Notes

The authors declare no competing financial interest.

ACKNOWLEDGMENTS

This work was supported by the Sino-Japanese Joint Research Platform on the Energy and Environmental Industry (no. 2017YFE0127100) and the KE JI XING MENG Project (no. 20H100000845). The authors thank the Instrumental Analysis Center of SJTU for help with analysis.

REFERENCES

(1) Sanger, A.; Kumar, A.; Kumar, A.; Jain, P. K.; Mishra, Y. K.; Chandra, R. Silicon Carbide Nanocauliflowers for Symmetric Supercapacitor Devices. *Ind. Eng. Chem. Res.* **2016**, *55*, 9452−9458.

(2) Ge, D.; Yang, L.; Fan, L.; Zhang, C.; Xiao, X.; Gogotsi, Y.; Yang, S. Foldable supercapacitors from triple networks of macroporous cellulose fibers, single-walled carbon nanotubes and polyaniline nanoribbons. *Nano Energy* **2015**, *11*, 568−578.

(3) Nam, I.; Kim, G.-P.; Park, S.; Han, J. W.; Yi, J. All-solid-state, origami-type foldable supercapacitor chips with integrated series circuit analogues. *Energy Environ. Sci.* **2014**, *7*, 1095−1102.

(4) Ma, L.; Bi, Z.; Zhang, W.; Zhang, Z.; Xiao, Y.; Niu, H.; Huang, Y. Synthesis of a Three-Dimensional Interconnected Oxygen-, Boron-, Nitrogen-, and Phosphorus Tetratomic-Doped Porous Carbon Network as Electrode Material for the Construction of a Superior Flexible Supercapacitor. *ACS Appl. Mater. Interfaces* **2020**, *12*, 46170−46180.

(5) Cheng, Y.; Huang, L.; Xiao, X.; Yao, B.; Yuan, L.; Li, T.; Hu, Z.; Wang, B.; Wan, J.; Zhou, J. Flexible and cross-linked N-doped carbon nanofiber network for high performance freestanding supercapacitor electrode. *Nano Energy* **2015**, *15*, 66−74.
(6) Yu, J.; Xie, F.; Wu, Z.; Huang, T.; Wu, J.; Yan, D.; Huang, C.; Li, L. Flexible metallic fabric supercapacitor based on graphene/polyaniline composites. *Electrochim. Acta* **2018**, *259*, 968−974.
(7) De, S.; Higgins, T. M.; Lyons, P. E.; Doherty, E. M.; Nirmalraj, P. N.; Blau, W. J.; Boland, J. J.; Coleman, J. N. Silver Nanowire Networks as Flexible, Transparent, Conducting Films: Extremely High DC to Optical Conductivity Ratios. *ACS Nano* **2009**, *3*, 1767−1774.
(8) Guo, X.; Zheng, S.; Zhang, G.; Xiao, X.; Li, X.; Xu, Y.; Xue, H.; Pang, H. Nanostructured graphene-based materials for flexible energy storage. *Energy Storage Mater.* **2017**, *9*, 150−169.
(9) Murugan, A. V.; Muraliganth, T.; Manthiram, A. Correction to Rapid, Facile Microwave-Solvothermal Synthesis of Graphene Nanosheets and Their Polyaniline Nanocomposites for Energy Strorage. *Chem. Mater.* **2010**, *22*, 2692.
(10) Kim, M.; Lee, C.; Jang, J. Fabrication of Highly Flexible, Scalable, and High-Performance Supercapacitors Using Polyaniline/Reduced Graphene Oxide Film with Enhanced Electrical Conductivity and Crystallinity. *Adv. Funct. Mater.* **2014**, *24*, 2489−2499.
(11) Song, N.; Wang, W.; Wu, Y.; Xiao, D.; Zhao, Y. Fabrication of highly ordered polyaniline nanocone on pristine graphene for high-performance supercapacitor electrodes. *J. Phys. Chem. Solids* **2018**, *115*, 148−155.
(12) Wu, Q.; Xu, Y.; Yao, Z.; Liu, A.; Shi, G. Supercapacitors based on flexible graphene/polyaniline nanofiber composite films. *ACS Nano* **2010**, *4*, 1963−1970.
(13) Yu, P.; Zhao, X.; Li, Y.; Zhang, Q. Controllable growth of polyaniline nanowire arrays on hierarchical macro/mesoporous graphene foams for high-performance flexible supercapacitors. *Appl. Surf. Sci.* **2017**, *393*, 37−45.
(14) Rong, L.; Ma, L.; Shu, H.; Jia, M.; Xu, J.; Yuan, G. A flexible polyaniline/graphene/bacterial cellulose supercapacitor electrode. *New J. Chem.* **2017**, *41*, 857−864.
(15) Luo, Z.; Lu, L.; Somers, L. A.; Johnson, A. T. C. High yield preparation of macroscopic graphene oxide membranes. *J. Am. Chem. Soc.* **2009**, *131*, 898−899.
(16) Wen, L.; Li, F.; Cheng, H.-M. Carbon Nanotubes and Graphene for Flexible Electrochemical Energy Storage: From Materials to Devices. *Adv. Mater.* **2016**, *28*, 4306−4337.
(17) Song, N.; Jia, J.; Wang, W.; Gao, Y.; Zhao, Y.; Chen, Y. Green production of pristine graphene using fluid dynamic force in supercritical CO2. *Chem. Eng. J.* **2016**, *298*, 198−205.
(18) Li, S.; Huang, D.; Zhang, B.; Xu, X.; Wang, M.; Yang, G.; Shen, Y. Flexible Supercapacitors Based on Bacterial Cellulose Paper Electrodes. *Adv. Energy Mater.* **2014**, *4*, 867−872.
(19) Schnepp, Z. Biopolymers as a Flexible Resource for Nanochemistry. *Angew. Chem.* **2013**, *52*, 1096−1108.
(20) Ma, L.; Bi, Z.; Xue, Y.; Zhang, W.; Huang, Q.; Zhang, L.; Huang, Y. Bacterial cellulose: An encouraging eco-friendly nano-candidate for energy storage and energy conversion. *J. Mater. Chem. A* **2020**, *8*, 5812−5842.
(21) Chen, L.; Huang, Z.; Liang, H.; Yao, W.; Yu, Z.; Yu, S. Flexible all-solid-state high-power supercapacitor fabricated with nitrogen-doped carbon nanofiber electrode material derived from bacterial cellulose. *Energy Environ. Sci.* **2013**, *6*, 3331−3338.
(22) Chen, W.; Yu, H.; Lee, S. Y.; Wei, T.; Li, J.; Fan, Z. Nanocellulose: A promising nanomaterial for advanced electrochemical energy storage. *Chem. Soc. Rev.* **2018**, *47*, 2837−2872.
(23) Ma, L.; Shi, C.; Zhao, N.; Bi, Z.; Guo, X.; Huang, Y. Bacterial cellulose based nano-biomaterials for energy storage applications. *J. Inorg. Mater.* **2020**, *35*, 145−157.
(24) Liu, R.; Ma, L.; Huang, S.; Mei, J.; Li, E.; Yuan, G. Large Areal Mass and High Scalable and Flexible Cobalt Oxide/Graphene/Bacterial Cellulose Electrode for Supercapacitors. *J. Phys. Chem. C* **2016**, *120*, 28480−28488.
(25) Ferrari, A. C.; Meyer, J. C.; Scardaci, V.; Casiraghi, C.; Lazzeri, M.; Mauri, F.; Piscanec, S.; Jiang, D.; Novoselov, K. S.; Roth, S. Raman spectrum of graphene and graphene layers. *Phys. Rev. Lett.* **2006**, *97*, No. 187401.
(26) Liu, Y.; Ma, Y.; Guang, S.; Ke, F.; Xu, H. Polyaniline-graphene composites with a three-dimensional array-based nanostructure for high-performance supercapacitors. *Carbon* **2015**, *83*, 79−89.
(27) Cai, Z.; Jin, H. J.; Kim, J. Chitosan blended bacterial cellulose as a smart material for biomedical application. *Proc. SPIE* **2009**, *7291*, No. 72910U.
(28) Asha, G.; Lata, S.; Kishore, N. Synthesis and structural characterization of polyaniline/cobalt chloride composites. *AIP Conf. Proc.* **2016**, *1731*, No. 140054.
(29) Ma, B.; Zhou, X.; Bao, H.; Li, X.; Wang, G. Hierarchical composites of sulfonated graphene-supported vertically aligned polyaniline nanorods for high-performance supercapacitors. *J. Power Sources* **2012**, *215*, 36−42.
(30) Feng, X.; Mao, C.; Yang, G.; Hou, W.; Zhu, J.-J. Polyaniline/Au composite hollow spheres: Synthesis, characterization, and application to the detection of dopamine. *Langmuir* **2006**, *22*, 4384−4389.
(31) Prabhu, S.; Vaideki, K.; Anitha, S. Effect of microwave argon plasma on the glycosidic and hydrogen bonding system of cotton cellulose. *Carbohydr. Polym.* **2017**, *156*, 34−44.
(32) Liu, Y.; Ma, Y.; Guang, S.; Xu, H.; Su, X. Facile fabrication of three-dimensional highly ordered structural polyaniline−graphene bulk hybrid materials for high performance supercapacitor electrodes. *J. Mater. Chem. A* **2014**, *2*, 813−823.
(33) Zhang, Q. E.; Zhou, A.; Wang, J.; Wu, J.; Bai, H. Degradation-induced Capacitance: A New Insight into the Superior Capacitive Performance of Polyaniline/Graphene Composites. *Energy Environ. Sci.* **2017**, *10*, 2372−2382.
(34) Darowicki, K.; Kawula, J. Dynamic electrochemical impedance spectroscopy of the adsorption and relaxation of polyaniline chains during potentiodynamic redox transformations. *Russ. J. Electrochem.* **2007**, *43*, 1055−1063.
(35) Gosser, D. K. Cyclic Voltammetry: Simulation and Analysis of Reaction Mechanisms. *Synth. React. Inorg. Met. − Org. Chem.* **1994**, *24*, 1237−1238.
(36) Xue, M.; Li, F.; Zhu, J.; Song, H.; Zhang, M.; Cao, T. Structure-Based Enhanced Capacitance: In Situ Growth of Highly Ordered Polyaniline Nanorods on Reduced Graphene Oxide Patterns. *Adv. Funct. Mater.* **2012**, *22*, 1284−1290.
(37) Shao, W.; Tebyetekerwa, M.; Marriam, I.; Li, W.; Wu, Y.; Peng, S.; Ramakrishna, S.; Yang, S.; Zhu, M. Polyester@MXene nanofibers-based yarn electrodes. *J. Power Sources* **2018**, *396*, 683−690.
(38) Ma, W.; Chen, S.; Yang, S.; Chen, W.; Weng, W.; Zhu, M. Bottom-up Fabrication of Activated Carbon Fiber for All-Solid-State Supercapacitor with Excellent Electrochemical Performance. *ACS Appl. Mater. Interfaces* **2016**, *8*, 14622−14627.
(39) Foo, C. Y.; Sumboja, A.; Tan, D. J. H.; Wang, J.; Lee, P. S. Flexible and Highly Scalable V_2O_5-rGO Electrodes in an Organic Electrolyte for Supercapacitor Devices. *Adv. Energy Mater.* **2014**, *4*, 3412−3420.
(40) Wu, X.; Wang, Q.; Zhang, W.; Wang, Y.; Chen, W. Nano nickel oxide coated graphene/polyaniline composite film with high electrochemical performance for flexible supercapacitor. *Electrochim. Acta* **2016**, *211*, 1066−1075.
(41) Xiao, X.; Li, T.; Yang, P.; Gao, Y.; Jin, H.; Ni, W.; Zhan, W.; Zhang, X.; Cao, Y.; Zhong, J.; Gong, L.; Yen, W.-C.; Mai, W.; Chen, J.; Huo, K.; Chueh, Y.-L.; Wang, Z. L.; Zhou, J. Fiber-Based All-Solid-State Flexible Supercapacitors for Self-Powered Systems. *ACS Nano* **2012**, *6*, 9200−9206.
(42) Feng, J.; Ye, S.; Lu, X.; Tong, Y.; Li, G. Asymmetric Paper Supercapacitor Based on Amorphous Porous Mn3O4 Negative Electrode and Ni(OH)2 Positive Electrode: A Novel and High-Performance Flexible Electrochemical Energy Storage Device. *ACS Appl. Mater. Interfaces* **2015**, *7*, 11444−11451.
(43) Zhang, Z.; Xiao, F.; Wang, S. Hierarchically structured MnO2/graphene/carbon fiber and porous graphene hydrogel wrapped

https://doi.org/10.1021/acsomega.1c00442
ACS Omega 2021, 6, 11427−11435

copper wire for fiber-based flexible all-solid-state asymmertric supercapacitors. *J. Mater. Chem. A* **2015**, *3*, 11215−11223.
(44) Lyu, S.; Chang, H.; Fu, F.; Hu, L.; Huang, J.; Wang, S. Cellulose-coupled graphene/polypyrrole composite electrodes containing conducting networks built by carbon fibers as wearable supercapacitors with excellent foldability and tailorability. *J. Power Sources* **2016**, *327*, 438−446.
(45) Yuan, L.; Yao, B.; Hu, B.; Huo, K.; Chen, W.; Zhou, J. Polypyrrole-coated paper for flexible solid-state energy storage. *Energy Environ. Sci.* **2013**, *6*, 470−476.

https://doi.org/10.1021/acsomega.1c00442
ACS Omega 2021, 6, 11427−11435